A novel pulmonary nodule classification framework based on mobile edge computing

Peng Wang*

ShangXi Eye Hospital,
Taiyuan 030002, China
Email: wangpengdepass@163.com
*Corresponding author

Zijuan Zhao

College of Information and Computer,
Taiyuan University of Technology,
Taiyuan 030024, China
Email: zhaozijuan0302@link.tyut.edu.cn

Abstract: Classification of benign and malignant pulmonary nodules is a critical task for developing a Computer-Aided Diagnosis (CAD) system of lung cancer. However, the intelligent diagnosis technology is often limited by equipment and space. Therefore, a computer-aided diagnosis model is proposed running in the Mobile Edge Computing (MEC) environment. The novel lung nodule classification framework improved the Deep Convolutional Generative Adversarial Nets (DCGAN). Firstly, CT images after pre-processing are input into GAN to generate new images with similar features. Then, in the training stage, the derivative model of GAN is introduced into the classification of pulmonary nodules. The optimised function means the improved DCGAN has better anti-noise ability and achieves more accurate classification performance. The experimental results showed an accuracy of 88.88%. Compared with the existing methods, the proposed method is superior to other ones in terms of accuracy, sensitivity, specificity, and area under the ROC curve.

Keywords: pulmonary nodules; generative adversarial nets; feature extraction; classification; mobile edge computing.

Reference to this paper should be made as follows: Wang, P. and Zhao, Z. (2020) 'A novel pulmonary nodule classification framework based on mobile edge computing', *Int. J. Wireless and Mobile Computing*, Vol. 18, No. 1, pp.80–89.

Biographical notes: Peng Wang is a Senior Engineer of ShangXi Eye Hospital, and a Systems Analyst. He received his Master degree of Software Engineering from Taiyuan University of Technology, Taiyuan, China. His current research topics include image processing, advantage and artificial intelligence.

Zijuan Zhao received her BS degree in Taiyuan University of Technology. She is currently pursuing her PhD degree in the area of Medical Image Processing and Artificial Intelligence at Taiyuan University of Technology.

1 Introduction

Mobile terminals, such as smartphones, tablets and net-books, are increasingly penetrating into our everyday lives as convenient tools for communication, entertainment, business, social networking, news, etc. However, such a growth in mobile wireless traffic is not matched by an equally fast improvement on mobile handsets' batteries, as testified in Sardellitti et al. (2015). Also, limitations of mobile devices such as privacy, resource limitations, and mobility take special requirements for computing power and data formats. The limited battery lifetime is also going to represent the stumbling block to the deployment of computation intensive applications for mobile devices.

However, in recent years, a new trend in computing is happening with the function of clouds being increasingly moving towards the network edges (Chiang and Zhang, 2016). Mobile Edge Computing (MEC) is emerging as a very promising computation architecture by pushing computation and storage closer to end users with both strategically deployed and opportunistic processing and storage resources (Mao et al., 2017). Harvesting the vast amount of the idle

computation power and storage space distributed at the network edges can yield sufficient capacities for performing computation-intensive and latency-critical tasks at mobile devices.

Mobile health aims to provide people with the medical information management and medical transaction processing in the form of Electronic Health (E-Health) applications by using mobile communication technologies and devices (Luckett et al., 2015; Luers et al., 2019). The biggest feature is to provide anytime, anywhere pervasive healthcare, which enables healthcare systems to allocate medical resources more effectively. In addition, lung cancer is the most common cause of death in both men and women, accounting for about 27% of all cancer deaths in cancer diseases (Siegel et al., 2015, 2018). The 5-year survival for patients with an early diagnosis is approximately 54%, as compared to 4% if the diagnosis is made late when the patient has the stage IV disease (Bach et al., 2012; Sun et al., 2016; Nishio and Nagashima, 2017; Firmino et al., 2016). Hence, the early screening and accurate diagnosis of lung nodules is extremely important. Using the application of mobile medicine and Deep Convolutional Generative Adversarial Nets (DCGAN), our work proposes a service architecture for mobile medical technology in the field of automatic classification of pulmonary nodules.

Owing the complex structure of the lungs, the shape and location of the nodules in different cases are different, and the doctors have great limitations only by the method of reading with the naked eye. At the same time, explosion of CT data takes the great challenge for doctors to give labels. Therefore, it is necessary to assist the doctor in the diagnosis of benign and malignant pulmonary nodules by means of the Computer-Aided Diagnosis (CAD) system (Suzuki et al., 2017). Recent advance of deep learning techniques has been shown to effectively address many medical image analysis problems like segmentation (Ronneberger et al., 2015; Cicek et al., 2016), lesion detection (Roth et al., 2014, 2015), differential diagnosis (Cheng et al., 2016; Shen et al., 2017), quality assessment (Wu et al., 2017), reference plane retrieve (Chen et al., 2017), etc. with perceivable performance improvement. Setio et al. (2016) used nine independent CNNs (with three convolution layers each) on different nodal views (axial, coronal, sagittal and six diagonal planes) to perform the classification and determine the existence of the nodules. The final classification results were obtained by fusing the CNN output with a fully connected layer. The deep learning techniques are equipped with the advantages of automatic feature learning, end-to-end training, etc. (Cui et al., 2018). And thus the steps of explicit feature engineering as well as other intermediate processing in the conventional pattern recognition framework can be circumvented. Therefore, the performance tuning of the deep learning techniques can be relatively simple and easy.

Figure 1 The overview of mobile-edge computing and classification of pulmonary nodules model

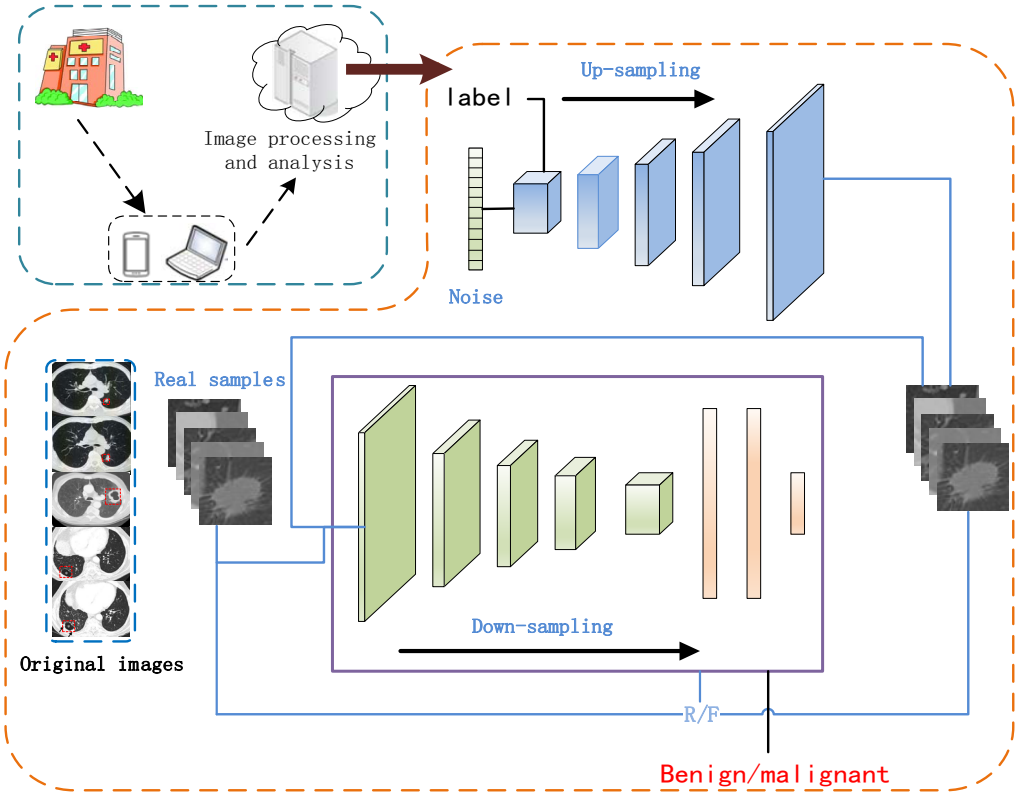

In this paper, we investigate the deep learning approach called Generative Adversarial Networks (GAN) (Goodfellow et al., 2014) to synthesise samples within general distribution-aware decision region for the minority classes to combat data imbalance problem. The family of the GAN techniques has been shown successfully in the applications of text-to-image (Reed et al., 2016; Han et al., 2017) as well as image-to-image translation (Isola et al., 2017), image super-resolution (Ledig et al., 2017), etc. In medical image analysis, the GAN technique was also introduced to synthesise images of different modality (Ledig et al., 2018; Zhang et al., 2018), denoising for low dose CT (Wolterink et al., 2017), segmentation (Dai et al., 2017), image reconstruction (Li et al., 2017), etc.

The GAN technique was firstly introduced by Goodfellow et al. (2014) and basically is constituted of two networks of a generator and a discriminator. The two networks are trained at the same time and compete against each other in a minimax game. The generator is trained to fool the discriminator by synthesising realistic samples, whereas the discriminator is trained to be equipped high discriminative capability for the synthetic samples. However, the training of the two networks can be quite unstable and may suffer mode collapse problem.

Aiming at the above problems, based on image processing technology and mobile computing environment, we applied a deep convolution generation antagonism model for malignancy classification of pulmonary nodules. The framework of mobile-edge computing and classification of pulmonary nodules model is show in Figure 1. The main innovations of this method include two aspects: (1) the derivative model of GAN is introduced into the classification of pulmonary nodules, that is, the deep convolution generation antagonism network model DCGAN is used to solve the problem of mode collapse; (2) the DCGAN model is improved and the model is modified. The optimised function gives the improved DCGAN better anti-noise ability in the process of image generation and realises accurate classification of benign and malignant pulmonary nodules. This method can enable physician and patients to obtain their information anytime and anywhere, and get rid of the constraints of time and space.

2 Mobile edge computing model

2.1 System model

We consider a mobile-edge cloud computing model as in Figure 2. We assume that the system consists of N MDs, an edge cloud located at the edge of the radio access networks, and a distant central cloud. Each MD executes an application and generates a series of homogeneous service requests. In this paper, we consider the queue model at MD as a *M/M/1* queue, the edge cloud as a *M/M/c* queue and the central cloud as a $M/M/\infty$ queue. For each MD, it can offload a portion or whole of its requests to edge cloud through a wireless channel, where the transmission suffers from interference generated by other MDs and noise power. If the total request rate is less than the maximum accepted rate of the edge cloud, then all the offloaded requests will be processed on the edge cloud. Otherwise, the edge cloud will further offload the overloaded requests to the central cloud for executing.

Figure 2 Mobile-edge cloud computing model

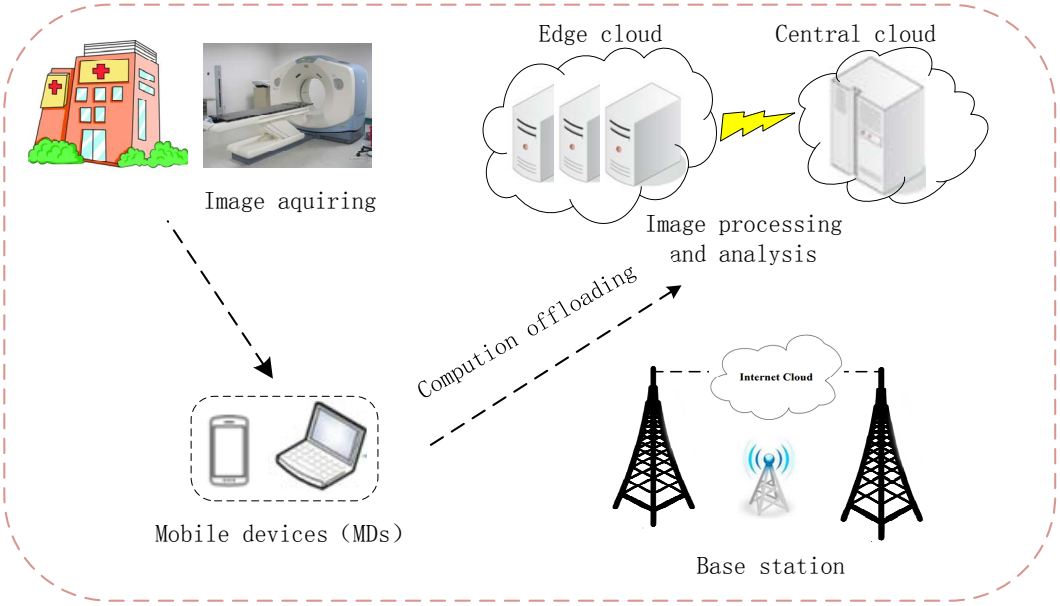

We assume that the requests generated by MD i, $i \in \{1,2,...,N\}$; N_g follows a Poisson process with an average arrival rate of λ_i. Each request generating from the MD i, $(i=1,2,...,N)$ contains a data size of θ_i. The MD chooses to offload the service request with a probability $p_i^C \left(0 \le p_i^C \le 1\right)$. We refer to p_i^C as the offloading probability of the MD i hereinafter. According to the properties of the Poisson distribution, the service requests which are offloaded to cloud follow a Poisson process with an average rate of $p_i^C \lambda_i$, the service requests which are processed locally also follow a Poisson process with average rate of $\left(1-p_i^C\right)\lambda_i$. In this paper, p_i^C $(i=1,2,...,N)$ are optimisation variable.

2.2 Local execution model and transmission

Let u_i^M denotes the computing capability of MD i. Additionally, we assume that l_i^M denotes the normalised workload on the MD i which represents the percentages of CPU that have been occupied. When considering a *M/M/1* queue, the response time of a *M/M/1* queue is $R=\dfrac{1/u}{1-p}$ (Lazar et al., 2003), where $\rho=\dfrac{\lambda}{u}$ is the queue utilisation, λ is the queue arrival rate, u is the service rate. Then the average response time T_i^M for locally processing requests at MD i is expressed as follows:

$$T_i^M\left(p_i^C\right)=\frac{1}{u_i^M\left(1-l_i^M\right)-\left(1-p_i^C\right)\lambda_i} \tag{1}$$

The MD i transmits the data to the edge cloud through wireless base station. Considering the mutual interference caused by other MDs and the background interference, we can compute the uplink data rate for computation offloading of MD i as follows (Chen et al., 2015):

$$R_i=W\log_2\left(1+\frac{P_iH_{i,s}}{\omega_i+\sum_{j\in N,j\neq i}P_jH_{j,s}}\right) \tag{2}$$

where W is the channel bandwidth and P_i is the transmission power of the MD i which are also the optimisation variable in this paper. Additionally, $0 < P_i \le P_i^{th}$, where P_i^{th} is the maximum transmission power of MD i. $H_{i,s}$ is the channel gain between the MD i and the base station. ω_i denotes the background interference power.

From the communication model in (2), we can compute the transmission time of MD i for offloading the data from MD i to the base station as follows (Chen et al., 2015):

$$T_i^t\left(p_i^C,P_i\right)=\frac{p_i^C\lambda_i\theta_i}{R_i}=\frac{p_i^C\lambda_i\theta_i}{W\log_2\left(1+\dfrac{P_iH_{i.s}}{\omega_i+\sum_{j\in N,j\neq i}P_jH_{j.s}}\right)} \tag{3}$$

The energy consumption $E_i^M p_i^C$ of local executing the requests for MD i can be given as follows (Barbarossa et al., 2014):

$$E_i^M\left(p_i^C\right)=\kappa_i T_i^M\left(p_i^C\right)=\kappa_i\frac{1}{u_i^M\left(1-l_i^M\right)-\left(1-p_i^C\right)\lambda_i} \tag{4}$$

where κ_i is the coefficient denoting the locally computation power of MD i.

We denote the energy consumption of transmitting the offloading requests from the MD to base station is $E_i^S\left(p_i^C\right)$, which can be given as follows (Chen et al., 2015):

$$\begin{aligned}E_i^s\left(p_i^C,P_i\right)&=P_iT_i^t\left(p_i^C\right)=P_i\frac{p_i^C\lambda_i\theta_i}{R_i}\\&=\frac{p_i^C\lambda_i\theta_i}{W\log_2\left(1+\dfrac{P_iH_{i.s}}{\omega_i+\sum_{j\in N,j\neq i}P_jH_{j.s}}\right)}\end{aligned} \tag{5}$$

2.3 Cloud execution model

Accordingly, we assume that there are c homogeneous servers deployed in the edge cloud, and the edge cloud is modelled as a $M/M/c$ queue. The service rate for each server is denoted as u^C. The maximum workload of the edge cloud is capped at a maximum request accepted rate denoted as $\lambda_{\max}^C$. The requests from different MDs in the system are pooled together with a total rate λ_{Total}^M which can be denoted as follows:

$$\lambda_{\text{Total}}^M=\sum_{i=1}^{N}\lambda_i p_i^C \tag{6}$$

Then the fraction of the requests ψ^C that the edge cloud can process can be expressed as equation (7). It means that if maximum workload of the edge cloud is more than the total rate from different MDs, the execution coefficient is 1. Otherwise, execution rate at the edge cloud depends on $\lambda_{\max}^C$.

$$\psi^C=\begin{cases}1, & \lambda_{\max}^C\ge\lambda_{\text{Total}}^M\\ \dfrac{\lambda_{\max}^C}{\lambda_{\text{Total}}^M}, & \lambda_{\max}^C<\lambda_{\text{Total}}^M\end{cases} \tag{7}$$

Correspondingly, the actual execution rate at the edge cloud is the product of ψ^C and $\lambda_{\max}^C$, which can be expressed as:

$$\lambda_p^C = \psi^C \lambda_{\text{Total}}^M = \begin{cases} \lambda_{Total}^M, \lambda_{\max}^C \geq \lambda_{\text{Total}}^M \\ \lambda_{\max}^C, \lambda_{\max}^C < \lambda_{\text{Total}}^M \end{cases} \tag{8}$$

To this end, based on the analysis of $M/M/c$ queue at the edge cloud and Erlang's Formula (Ngo and Lee, 1990), we define:

$$\rho^C = \frac{\lambda_p^C}{cu^C} \tag{9}$$

Therefore, the average waiting time of each request at the edge cloud, which contains the queuing time and execution time, is denoted as follows:

$$T_{wait}^C = \left(\lambda_p^C\right) = \frac{C\left(c,\rho^C\right)}{cu^C - \lambda_p^C} + \frac{1}{u^C} \tag{10}$$

where

$$C\left(c,\rho^C\right) = \frac{\left(\frac{\left(c\rho^C\right)}{c!}\right)\left(\frac{1}{1-\rho^C}\right)}{\sum_{k=0}^{c-1}\frac{\left(c\rho^C\right)^k}{k!} + \left(\frac{\left(c\rho^C\right)}{c!}\right)\left(\frac{1}{1-\rho^C}\right)} \tag{11}$$

Assuming u_b^C is the transmission rate of the edge cloud, we can obtain the expected time T_b^C for the execution results waiting in the edge cloud before they are completely delivered out as follows:

$$T_b^C\left(\lambda_p^C\right) = \frac{1}{u_b^C - \lambda_p^C} \tag{12}$$

The overloaded requests are transmitted to the central cloud through wired connection which incurs a fixed time delay T^O. As the central cloud is considered as $M/M/\infty$ with the service rate u^{CC}. Then, the waiting time T_{wait}^{CC} of overloaded request can be presented as follows:

$$T_{wait}^{CC} = T^O + \frac{1}{u^{CC}} \tag{13}$$

The expected time *TCC b* for the results waiting in the cloud before they are completely sent out is denoted as

$$T_{wait}^{CC}\left(p_i^C\right) = \frac{1}{u_b^{CC} - \left(\lambda_{\text{Total}}^M - \lambda_p^C\right)} \tag{14}$$

We neglect the time and energy consumption for the MD to receive the processed outcome, which is similar to previous work (Chen et al., 2015).

3 Classification method

3.1 Generative adversarial nets

In this study, the technique of the Generative Adversarial Networks (GAN) is employed for the over-sampling of the minority subordinate classes. Typical GAN can comprise a generator and a discriminator network. The functionality of the generator network is to synthesise samples by estimating the underlying distribution of the target domain, whereas the discriminator aims to differentiate the true samples and the synthetic samples derived from the generator. The optimisation process of the GAN pushes the generator to synthesise plausible samples that can fool the discriminator, while also sharpens the differentiation capability of the discriminator. Therefore, the effective training of the GAN needs to optimise two networks. The concept of the typical GAN is illustrated in Figure 3.

Figure 3 GAN network model

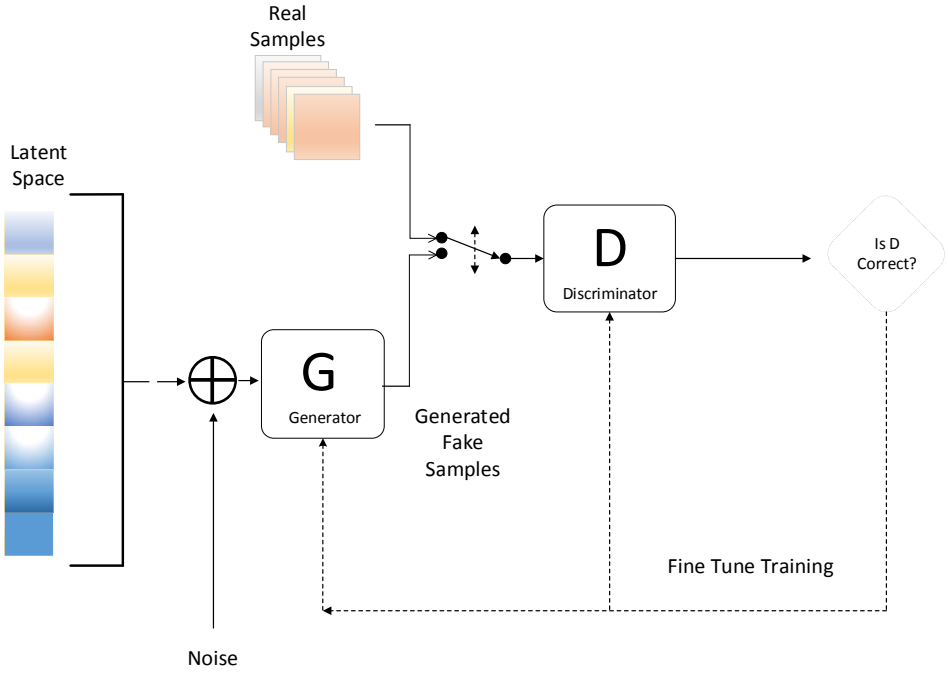

Since it needs to train the networks of the generator and discriminator for the GAN, the optimisation process can be difficult and may suffer several drawbacks. First, the training of the GAN is relatively unstable and may highly depend on the competition between the generator and the discriminator within the minimax game framework. In other words, a good equilibrium between the generator and the discriminator is important to yield good quality of sample synthesise. However, the gradient descent during the training of the networks can't always promise a good equilibrium. For example, if a discriminator is equipped with high differentiation capability in the training process, the generator's gradient may vanish quickly. Therefore, the optimisation of the generator may not be able to proceed to approximate the true distribution of the target domain. As suggested by Goodfellow et al. (2014), a better generator can be trained if the discriminator is deliberately weaken. In such case, it may then require several passes of trial and error and turn the whole training process difficult and unstable. Second, there exists the so-called mode collapse in GAN, where the generator tends to produce samples with low variety. The mode collapse is caused by the cases that the generator is trapped to the same local minimum of the cost function to synthesise similar samples. In such case, the generated samples are not sufficiently diverse to represent the whole distribution of the target domain, and hence are not helpful to address the problem of the data imbalance.

3.2 Deep convolutional generative adversarial nets – DCGAN

Radford et al. (2015) pointed out that due to the lack of representative feature learning process and heuristic loss function, the GAN model is unstable, difficult to train and easy to collapse. Therefore, a deep convolution generation is proposed against the network DCGAN model. The DCGAN model is a derivative model of GAN, The CNN structure (Cui et al., 2019) is used to extend the structure of the *G* model and the *D* model in GAN, with the following modifications: (1) Cancel all pooling layers of CNN. G uses partial cross-convolution instead of pooling layer, and *D* uses cross-convolution instead of pooling layer. (2) Cancel the Full Connection layer (FC layer) of CNN and make the network become full convolution network. (3) Use ReLU as the activation function in *G*, and use the tanh function as the activation function in the output layer; in model *D*, the activation function for all layers is the Leaky ReLU function. (4) Using a batch lung nodule image as input, the input parameters of *G* are the noise *z* and the label category of the lung nodule image *c*; the input parameters of *D* are a fixed-size true lung nodule image and a lung nodule image generated by *G*.

In order to make full use of the CNN network structure to extract the unique advantages of the texture features of the lung nodules of the two-dimensional CT image and the function of the GAN to generate images, It also solves the problem of imbalance in the proportion of benign and malignant samples of lung nodules when training CNN, and prevents the instability of network model when training GAN, difficult to train and easy to collapse. In the early diagnosis of pulmonary nodules, this paper first introduced DCGAN model. DCGAN model has the following advantages: it can generate pulmonary nodules with similar texture characteristics to the input image according to the input pulmonary nodule image, and to generate images for training the DCGAN model, so as to solve the problem of insufficient samples of malignant pulmonary nodules. Moreover, the CNN convolution structure can be used to solve the instability problem and difficult training problems of GAN model. At the same time, DCGAN has the following problems in the application of pulmonary nodules: (1) The images generated by *G* model in DCGAN are liable to be blurred due to the influence of noise points, that is, the ability of anti-noise is weak. (2) In the DCGAN, the *D* model can only classify the input lung nodule images, and cannot classify the lung nodules.

3.3 Improved deep convolutional generative adversarial nets

In order to solve the problems in the diagnosis of early pulmonary nodules in the original DCGAN, improve the DCGAN model, modify the optimisation function of the DCGAN model, and improve the discriminant function of the DCGAN model: change the data source classification problem to data source classification and lung node good and bad classification problems. Improved DCGAN includes a *G* and a *D*. Like the original DCGAN, G generates lung nodule images with similar texture features to the input image based on the input noise and image categories. The difference from the original DCGAN: (1) When inputting an image in the *D* model, the category label corresponding to the image is also used as the input of the *D* model; (2) *D* has two parts in the discriminating process, classifying the source of the input image, and classifying the input image. The comparison between the original DCGAN and the improved DCGAN framework is shown in Figure 4. The optimisation function of the improved DCGAN network model is modified into two parts: Logarithmic function L_s of image source and logarithmic function L_c of image category. In the process of training G, G maximises $L_c - L_s$ as much as possible, that is, maximises the discriminative power of the tag category, and minimises the discriminative power of the source. In the process of training D, D maximises $L_c + L_s$ as much as possible, that is, maximises the discriminative power of the label category and maximises the discriminative power of the source. The logarithmic function L_s of the image source is as shown in equation (15). The logarithmic function of the image label class L_c is as shown in equation (16) (Setio et al., 2016):

$$L_s = E_{x\sim P_{data}}(x)\lg S(x) + E_{x\sim P_z(z)}\lg S\left(G\left(c,z\right)\right) \tag{15}$$

$$L_c = E_{x\sim P_{data}}(x)\lg C(x) + E_{x\sim P_z(z)}\lg C\left(G\left(c,z\right)\right) \tag{16}$$

Figure 4 Comparison of DCGAN architecture and improved DCGAN architecture

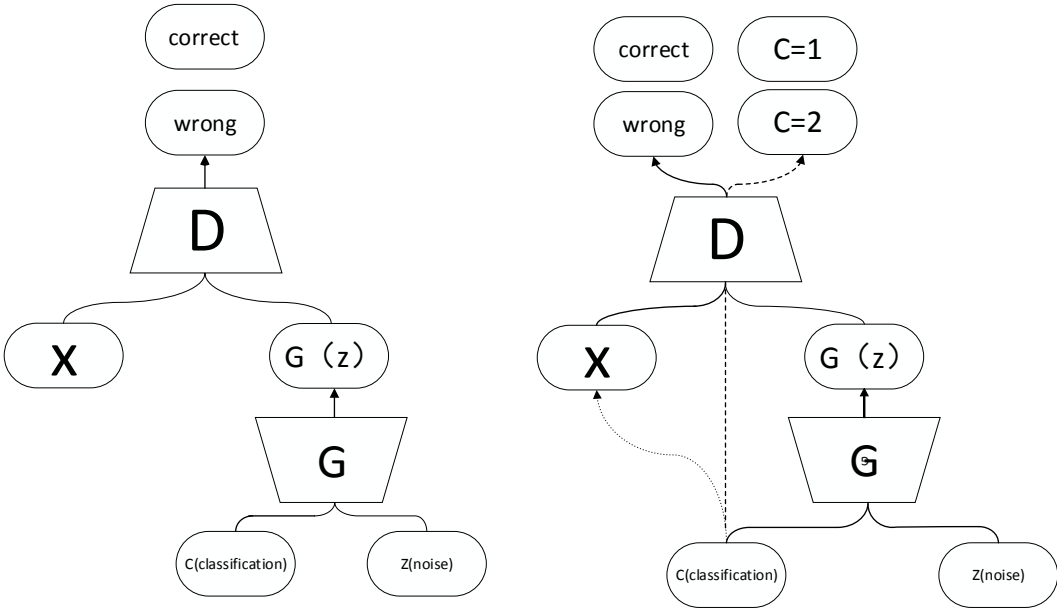

Among them: x represents the true lung nodule image; z represents the noise of input G; c indicates the type of label that G produces for the lung nodule image. $G(c, z)$ represents the lung nodule image generated by G; $S(x)$ denotes the probability of D judging the real pulmonary nodule image as image x. $S(G(c, z))$ denotes the probability that D judges G to generate image $G(c, z)$ as image x. If the input image is derived from image x, the probability is 1; If the input image is derived from the image G generated by $G(c, z)$, the probability is 0. $C(x)$ indicates the probability that D classifies whether image x is correct, and $C(G(c, z))$ indicates the probability that D is the correct classification of image $G(c, z)$. If the input image is classified correctly, the probability is 1; if the input image is classified incorrectly, the probability is 0.

When the input noise z conforms to the probability distribution pz ,the probability distribution pg is the probability distribution formed by G for the generated image $G(c, z)$.When a sufficient number of lung nodule images are input, Algorithm 1 finally converges to an estimate of the image x probability distribution P_{data} .

Algorithm 1: Improved DCGAN model training with stochastic gradient degree method

Input: Small batch data m noise points $\left\{z^{(1)},...,z^{(m)}\right\}$

Small batch data with m real pulmonary nodule images $\left\{x^{(1)},...,x^{(m)}\right\}$

Output: $D(x)$ = argmaxlgC(x). Enter the classification probability value of the lung nodule image.

Process:

For iteration rounds $n = 1, 2, ..., N$ **do**

For step k **do**

The small batch data has m noise points $\left\{z^{(1)},...,z^{(m)}\right\}$, The probability distribution is $\mathrm{P_g}(Z)$;

Small batch data with m real images $\left\{x^{(1)},...,x^{(m)}\right\}$, The probability distribution is $P_{data}(Z)$;

When updating the discriminant model D, add a random gradient:

$$\tilde{N}_{\theta_d}\frac{1}{m}\sum_{i=1}^{m}\left[\lg C\left(x^{(i)}\right)+\lg C\left(G\left(c^{(i)},z^{(i)}\right)\right)+\lg S\left(x^{(i)}\right)+\lg\left(G\left(c^{(i)},z^{(i)}\right)\right)\right]$$

end for

Small batch data with m noise points $\left\{z^{(1)},...,z^{(m)}\right\}$, The probability distribution is $P_g(Z)$;

When the generated model G is updated, the random gradient is subtracted:

$$\nabla_{\theta_g}\frac{1}{m}\sum_{i=1}^{m}\left[\lg C\left(G\left(c^{(i)},z^{(i)}\right)\right)-\lg S\left(G\left(c^{(i)},z^{(i)}\right)\right)\right]$$

end for

4 Experiments

4.1 Data set description

This experiment was performed based on data from 1018 sets of chest CT images from LIDC-IDRI database, which was initiated by the National Cancer Institute (NCI), further promoted by the National Institutes of Health Foundation (FNIH) and actively participated by the Food and Drug Administration (FDA), making it the largest open source image database of lung nodules (Armato et al., 2011).

The LIDC-IDRI database contains 1010 sets of medical records and 1018 sets of chest CT images. There are 244,527 chest CT images, each of which is marked by four experienced radiologists. The mark information is stored in XML format, including contour coordinates and malignancy of lung nodules. Radiologists quantify the malignancy (M) of lung nodules into five grades: 1, 2, 3, 4, and 5, indicating extreme impossibility, moderate impossibility, uncertainty, moderate suspicion and high suspicion.

4.2 Experimental program

This article uses the lung image public data set LIDC-IDRI, in which the size of the lung nodules is 3 to 30 mm, and the pixel level ranges from 6*6 to 60*60 pixels, in order to ensure batch training and data under large-scale data. Original, adjust the picture to 32*32. In order to improve the accuracy, the malignant nodules marked by at least three physicians were selected, to obtain the mean value. The mean value lower than 3 represented the benign nodules; the mean value higher than 3 represented the malignant nodules; and the nodules with a mean value of 3 were discarded. A total of 1265 nodules were obtained, including 779 benign nodules and 486 malignant nodules. In order to enhance the data set, the pre-processed ROI images were rotated by 90º, 180º and 270º, and flipped horizontally and vertically. Through 10-fold cross validation, data sets were divided into 10 groups, each of which was validated once.

4.3 Evaluation criterion

Accuracy, sensitivity, specificity and ROC curve are usually used as evaluation indicators in classification experiments of lung nodules (Nibali et al., 2017). The formula for evaluating the classification index is shown in Table 1, where TP represents true positive, TN represents true negative, FP represents false positive, and FN represents false negative. ROC curve refers to the receiver operating characteristic curve, which is a comprehensive index reflecting the continuous variables of sensitivity and specificity. The larger the area under the curve is, the higher the diagnostic accuracy will be. This is the most commonly used method (Bradley, 1997; Ling et al., 2003) for classification algorithms used to test machine learning performance. Finally, the experimental results would be given in the form of mean and standard deviation on the basis of repeated operation.

Table 1 Calculation formulas of evaluation index

Evaluation index	*Calculation formulas*
Accuracy (AC)	(TP+TN)/(TP+FP+FN+TN)
Sensitivity (SE)	TP/(TP+FN)
Specificity (SP)	FN/(TP+FN)

4.4 Performance comparison

The original DCGAN model and the improved DCGAN model use the test data set to verify the ability of the G model to generate images after training. Table 2 shows the corresponding image results generated by the G model based on the input image. As can be seen from Table 2, the improved DCGAN model can generate a corresponding level of image according to the label of the input image, and the generated image has 91.80%. The image is discriminated as a real image. It shows that the G model in DCGAN has better anti-noise ability when generating images, that is, the G model has very good generating ability.

Table 2 Source classification of samples from improved DCGAN

classification	*True*	*False*	*Total*	*ACC/%*
benign	1141	105	1246	91.57
malignant	717	61	778	92.16
Total	1858	166	2024	91.80

Test data sets were used to test the discriminant ability of D model in improved DCGAN. The results of classification of pulmonary nodules by improved DCGAN D model were shown in Table 3. From Table 3, it can be seen that the improved DCGAN can distinguish the benign and malignant images of pulmonary nodules on the test data sets, and the classification accuracy is 88.88%.

Table 3 Lung nodule images classification with improved DCGAN

Classification	*Predicted Benign*	*Predicted Malignant*	*Total*	*ACC/%*
benign	1087	159	1246	87.24
malignant	66	712	778	91.52
Total	1153	871	2024	88.88

In order to evaluate the performance of the proposed improved DCGAN model, it was compared with the recently published paper using the LIDC data set based on lung nodule depth learning classification method, and the results are shown in Table 4 and Figure 5.

As can be seen from Table 4, the Imp-DCGAN model has better lung nodule classification performance than other methods. Compared with the original DCGAN method, the accuracy of the Imp-DCGAN model proposed in this paper

is 1.95. Compared with the convolutional neural network, the accuracy is improved by 2.42. Compared with the classical GAN network, the accuracy is significantly improved, which is 5.24. It is fully explained that the optimisation function of modifying the DCGAN model can improve the classification accuracy of the network model.

Table 4 Comparisons of different algorithms for pulmonary nodules classification based on LIDC data set

Classification model	*AC+SD*	*SE+SD*	*SP+SD*
Setio-CNN	86.46±4.03	87.91±3.84	84.52±3.63
GAN	83.64±4.15	84.24±3.64	81.92±4.15
DCGAN	86.93±2.73	88.16±3.17	85.17±3.93
Imp-DCGAN	88.88±2.75	91.21±2.84	86.18±3.72

Figure 5 ROC curves for each model

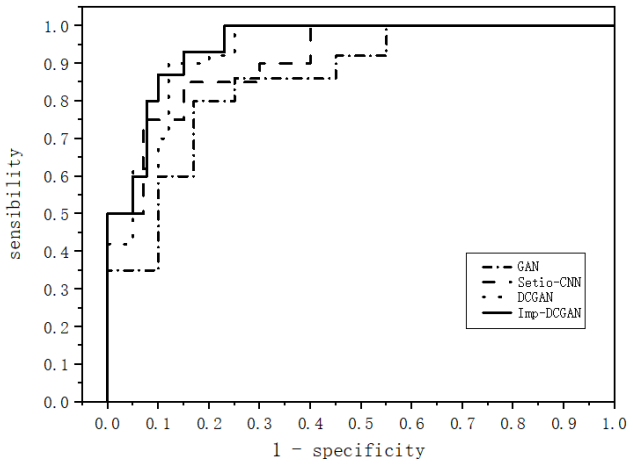

As can be seen from Figure 5, there are some differences in the results of different diagnostic methods. The ROC curve of this method is closer to the upper left of the coordinates than other methods, and the AUC value is the largest. It has obvious advantages in the diagnosis of benign and malignant pulmonary nodules.

5 Conclusion

In this paper, an improved DCGAN model is proposed to achieve the automatic classification of lung nodules. At the same time a convenient serve framework using mobile edge computing is designed for doctors and patients to get their diagnosis data any time anywhere. Our DCGAN model is improved from the traditional DCGAN model, improves the clarity of the images generated by G model in DCGAN, and solves the problem that D model in DCGAN can only classify the source of the input pulmonary nodule images, but cannot classify the benign and malignant pulmonary nodules. To a certain extent, it improves the accuracy of classification of benign and malignant pulmonary nodules. Experiments show that the proposed classification method of pulmonary nodules based on the improved deep convolution generation antagonism network is superior to the traditional generation antagonism network and the traditional deep learning classification algorithm.

References

Armato, S.G., Mclennan, G., Bidaut, L. et al. (2011) 'The lung image database consortium (LIDC) and image database resource initiative (IDRI): a completed reference database of lung nodules on CT scans', *Academic Radiology*, Vol. 14, No. 12, pp.1455–1463.

Bach, P.B., Mirkin, J.N., Oliver, T.K. et al. (2012) 'Benefits and harms of CT screening for lung cancer: a systematic review', *JAMA the Journal of the American Medical Association*, 307, No. 22, pp.2418–2429.

Barbarossa, S., Sardellitti, S. and Lorenzo, P.D. (2014) 'Communicating while computing: distributed mobile cloud computing over 5G heterogeneous networks', *IEEE Signal Processing Magazine*, Vol. 31, No. 6, pp.45–55.

Bradley, A.P. (1997) 'The use of the area under the ROC curve in the evaluation of machine learning algorithms', *Elsevier Science Inc.*, Vol. 30, No. 7, pp.1145–1159.

Chen, H., Wu, L., Dou, Q. et al. (2017) 'Ultrasound standard plane detection using a composite neural network framework', *IEEE Transactions on Cybernetics*, Vol. 47, No. 6, pp.1576–1586.

Chen, X., Jiao, L., Li, W.Z. and Fu, X.M. (2015) 'Efficient multiuser computation offloading for mobile-edge cloud computing', *IEEE/ACM Transactions on Networking*, in press, DOI: 10.1109/TNET.2015.2487344.

Cheng, J.Z., Ni, D., Chou, Y.H. et al. (2016) 'Computer-aided diagnosis with deep learning architecture: applications to breast lesions in US images and pulmonary nodules in CT scans', *Scientific Reports*, Vol. 6, pp.1–13.

Chiang, M. and Zhang, T. (2016) 'Fog and IoT: an overview of research opportunities', *IEEE Internet Things Journal*, Vol. 3, No. 6, pp.854–864.

Cicek, O., Abdulkadir, A., Lienkamp, S.S., Brox, T. and Ronneberger, O. (2016) *3D U-Net: Learning Dense Volumetric Segmentation from Sparse Annotation*, Springer, Cham, Switzerland, pp.424–432.

Cui, Z., Du, L., Wang, P., Cai, X. and Zhang, W. (2019) 'Malicious code detection based on CNNs and multi-objective algorithm', *Journal of Parallel and Distributed Computing*, Vol. 129, pp.50–58.

Cui, Z., Xue, F., Cai, X., Cao, Y., Wang, G. and Chen, J. (2018) 'Detection of malicious code variants based on deep learning', *IEEE Transactions on Industrial Informatics*, Vol. 14, No. 7, pp.3187–3196.

Dai, W. et al. (2017) *SCAN: Structure correcting adversarial network for organ segmentation in chest X-rays*. Available online at: https://arxiv.org/abs/1703.08770v1

Firmino, M., Angelo, G. and Morais, H. et al. (2016) 'Computer-aided detection (CADe) and diagnosis (CADx) system for lung cancer with likelihood of malignancy', *BioMedical Engineering OnLine*, Vol. 15, No. 1, pp.1–17.

Goodfellow, I.J., Pouget-Abadie, J. and Mirza, M. et al. (2014) 'Generative adversarial nets', *International Conference on Neural Information Processing Systems (NIPS)*, Vol. 2, pp.2672–2680.

Han, Z., Tao, X. and Li, H. (2017) 'StackGAN: text to photo-realistic image synthesis with stacked generative adversarial networks', *Proceedings of the IEEE International Conference on Computer Vision*, IEEE, Italy, pp.5908–5916.

Isola, P., Zhu, J.Y. and Zhou, T. et al. (2017) 'Image-to-image translation with conditional adversarial networks', *Proceedings of the Computer Vision and Pattern Recognition*, pp.5967–5976.

Lazar, A. (2003) 'The throughput time delay function of an M/M/1 queue (Corresp.)', *IEEE Transactions on Information Theory*, Vol. 29, No. 6, pp.914–918.

Ledig, C. et al. (2017) 'Photo-realistic single image super-resolution using a generative adversarial network', *Proceedings of the IEEE Computer Vision and Pattern Recognition (CVPR)*, pp.105–114.

Ledig, C., Theis, L. and Huszar, F. et al. (2018) 'Medical image synthesis with deep convolutional adversarial networks', *IEEE Transactions on Biomedical Engineering*, Vol. 65, No. 12, pp.2720–2730.

Li, Z., Wang, Y. and Yu, J. (2017) 'Reconstruction of thin-slice medical images using generative adversarial network', *International Workshop on Machine Learning in Medical Imaging*, Springer, Cham.

Ling, C.X, Huang, J. and Zhang, H. (2003) 'AUC: a better measure than accuracy in comparing learning algorithms', *Canadian Society for Computational Studies of Intelligence Conference on Advances in Artificial Intelligence,* Springer-Verlag, pp.329–341.

Luckett, D.J., Laber, E.B. and Kahkoska, A.R. et al. (2015) 'Estimating dynamic treatment regimes in mobile health using V-learning', *Journal of the American Statistical Association*, pp.1–39.

Luers, B., Klasnja, P. and Murphy, S. (2019) 'Standardized effect sizes for preventive mobile health interventions in micro-randomized trials', *Prevention Science*, Vol. 20, No. 1, pp.100–109.

Mao, Y., You, C. and Zhang, J. et al. (2017) 'Mobile edge computing: survey and research outlook', *IEEE Communications Surveys and Tutorials*, pp.1–31.

Ngo, B. and Lee, H. (1990) 'Analysis of a pre-emptive priority M/M/c model with two types of customers and restriction', *Electronics Letters*, Vol. 26, No. 15, pp.1190–1192.

Nibali, A, He, Z. and Wollersheim, D. (2017) 'Pulmonary nodule classification with deep residual networks', *International Journal of Computer Assisted Radiology and Surgery*, Vol. 12, No. 10, pp.1–10.

Nishio, M. and Nagashima, C. (2017) 'Computer-aided diagnosis for lung cancer: usefulness of nodule heterogeneity', *Academic Radiology*, Vol. 24, No. 3, pp.328–336.

Radford, A., Metz, L. and Chintala, S. (2015) 'Unsupervised representation learning with deep convolutional generative adversarial networks', *Computer Science*, Vol. 1, No. 1, pp.1–19.

Reed, S., Akata, Z., Yan, X., Logeswaran, L., Schiele, B. and Lee, H. (2016) 'Generative adversarial text to image synthesis', *Proceedings of the 33rd International Conference on Machine Learning (ICML JMLR)*, Vol. 48, pp.1060–1069.

Ronneberger, O., Fischer, P. and Brox, T. (2015) 'U-Net: convolutional networks for biomedical image segmentation', *International Conference on Medical Image Computing and Computer-assisted Intervention*, Springer, Cham, Switzerland, pp.234–241.

Roth, H.R. et al. (2014) 'A new 2.5D representation for lymph node detection using random sets of deep convolutional neural network observations', *Medical Image Computing and Computer-Assisted Intervention (MICCAI*), pp.520–527.

Roth, H.R., Lu, L. and Liu, J. et al. (2015) 'Improving computer-aided detection using convolutional neural networks and random view aggregation', *IEEE Transactions on Medical Imaging*, Vol. 35, No. 5, pp.1170–1181.

Sardellitti, S., Scutari, G. and Barbarossa, S. (2015) 'Joint optimization of radio and computational resources for multicell mobile-edge computing', *IEEE Transactions on Signal and Information Processing over Networks*, Vol. 1, No. 2, pp.89–103.

Setio, A.A., Ciompi, F. and Litjens, G. et al. (2016) 'Pulmonary nodule detection in CT images: false positive reduction using multi-view convolutional networks', *IEEE Transactions on Medical Imaging*, Vol. 35, No. 5, pp.1160–1169.

Shen, W., Zhou, M. and Yang, F. et al. (2017) 'Multi-crop convolutional neural networks for lung nodule malignancy suspiciousness classification', *Pattern Recognition*, Vol. 61, No. 61, pp.663–673.

Siegel, R.L. et al. (2018) 'Cancer statistics', *CA: a Cancer Journal for Clinicians*, Vol. 68, No. 1, pp.7–30.

Siegel, R.L., Miller, K.D. and Jemal, A. (2015) 'Cancer statistics', *Ca: A Cancer Journal for Clinicians*, Vol. 65, No. 1, pp.5–29.

Sun, W., Tseng, T-L., Zhang, J. and Qian, W. (2016) 'Computerized breast cancer analysis system using three stage semi-supervised learning method', *Computer Methods and Programs in Biomedicine*, Vol. 135, pp.77–88.

Suzuki, K. (2017) 'Computer-aided detection of lung cancer: image-based computer-assisted', *Radiation Therapy*, pp.9–40.

Wolterink, J.M., Leiner, T., Viergever, M.A. and Išgum, I. (2017) 'Generative adversarial networks for noise reduction in low-dose CT', *IEEE Transactions on Medical Imaging*, Vol. 36, No. 12, pp.2536–2545.

Wu, L., Cheng, J.Z. and Li, S. et al. (2017) 'FUIQA: Fetal ultrasound image quality assessment with deep convolutional networks', *IEEE Transactions on Cybernetics*, Vol. 47, No. 5, pp.1336–1349.

Zhang, Y., Cheng, J-Z., Xiang, L., Yap, P-T., Shen, D., Frangi, A.F., Schnabel, J.A., Davatzikos, C. Alberola-López, C. and Fichtinger, G. (2018) 'Dual-domain cascaded regression for synthesizing 7T from 3T MRI', *in Medical Image Computing and Computer Assisted Intervention – MICCAI*, Springer, Cham, Switzerland, pp.410–417.